Classification-driven stochastic watershed. Application to multispectral segmentation

Guillaume Noyel, Jesús Angulo, Dominique Jeulin; Centre de Morphologie Mathématique, Ecole des Mines de Paris; 35 rue Saint-Honoré, Fontainebleau, F - 77305, France: {guillaume.noyel, jesus.angulo, dominique.jeulin}@ensmp.fr

Abstract

The aim of this paper is to present a general methodology based on multispectral mathematical morphology in order to segment multispectral images. The methods consists in computing a probability density function pdf of contours conditioned by a spectral classification. The pdf is conditioned through regionalized random balls markers thanks to a new algorithm. Therefore the pdf contains spatial and spectral information. Finally, the pdf is segmented by a watershed with seeds (i.e. markers) coming from the classification.

Consequently, a complete method, based on a classification-driven stochastic watershed is introduced. This approach requires a unique and robust parameter: the number of classes which is the same for similar images.

Moreover, an efficient way to select factor axes, of Factor Correspondence Analysis (FCA), based on signal to noise ratio on factor pixels is presented.

Keywords: Stochastic Watershed, multispectral images, regionalized random balls, classification-driven stochastic watershed, marginal probability density function.

Introduction

Watershed transformation (WS) requires, for image segmentation, a function to flood, generally the norm of a gradient (i.e. a scalar function), and seeds (markers) for each region of interest [2]. This powerful approach is a deterministic process which tends to build irregular contours. The stochastic watershed was proposed in order to regularize and to produce more significant contours [1]. The initial framework was then extended to multispectral images [9].

The aim of this paper is to introduce improvements of the stochastic watershed and to compare them with the segmentations obtained with the deterministic WS for multispectral images.

The standard stochastic watershed starts from uniform random point markers to flood the norm of a gradient, in order to obtain associated contours to random markers. After repeating the process a large number of times, a probability density function of contours (pdf) is computed by the Parzen kernel method. In our previous works, this pdf was segmented by hierarchies based on extinction values (according to dynamics, surface and volume) in order to select the most significant minima of the pdf. The selected minima were used as the markers for the watershed [7]. In the case of multispectral images, a pdf is built for each channel of the image and the flooding function is the weighted sum of the channels pdf. This function is called a weighted marginal probability density function $mpdf$ [9].

In this paper, we generate the pdf using the results of a prior classification. First, we compute a spectral classification of the multispectral image by unsupervised approaches such as "k-means" or "clara" [11]. After filtering each class, we obtain some seeds s used as markers to segment the flooding function. This function is a pdf in the stochastic case, or a multivariate gradient in the deterministic one [8].

The main contributions of this paper are the new algorithm to build the pdf conditionally to the classification, and the segmentation of the pdf with seeds (i.e. markers) obtained by the classification. Finally, we propose a full treatment chain for multispectral images with a robust parameter: the number of classes for the classification.

The method presented here can be applied in various multispectral image fields: remote sensing, microscopy images, medical images [10], thermal images, temporal series, multivariate series, etc.

Multispectral image space (MIS) vs. factor image space (FIS)

Multispectral images are multivariate discrete functions with typically several tens or hundreds of spectral bands. In a formal way, each pixel of a multispectral image is a vector with values in wavelength, in time, or associated with any index j. To each wavelength, time or index corresponds an image in two dimensions called channel. In the sequel, we use only the term of spectrum and spectral channel. The number of channels depends on the nature of the specific problem under study (satellite imaging, spectroscopic images, temporal series, etc.). Let

$$\mathbf{f}_\lambda : \left\{ \begin{array}{lcl} E & \rightarrow & \mathscr{T}^L \\ x & \rightarrow & \mathbf{f}_\lambda(x) = \left(f_{\lambda_1}(x), f_{\lambda_2}(x), \ldots, f_{\lambda_L}(x)\right) \end{array} \right. \quad (1)$$

be an hyperspectral image, where:

- $E \subset \mathbb{R}^2$, $\mathscr{T} \subset \mathbb{R}$ and $\mathscr{T}^L = \mathscr{T} \times \mathscr{T} \times \ldots \times \mathscr{T}$
- $x = x_i \setminus i \in \{1,2,\ldots,P\}$ is the spatial coordinates of a vector pixel $\mathbf{f}_\lambda(x_i)$ (P is the pixels number of E)
- $f_{\lambda_j} \setminus j \in \{1,2,\ldots,L\}$ is a channel (L is the channels number)
- $f_{\lambda_j}(x_i)$ is the value of vector pixel $\mathbf{f}_\lambda(x_i)$ on channel f_{λ_j}.

Due to the redundancy of channels, a data reduction is usually performed using Factor Correspondence Analysis (FCA) [4]. We prefer a FCA in place of a Principal Component Analysis (PCA), because image values are positive and the spectral channels can be considered as probability distributions. As for PCA, from selected factorial FCA axes the image can be partially reconstructed. The metric used in FCA is the chi-squared, which is adapted to probability laws and normalized by channels weights. FCA can be seen as a transformation going from image space to factorial space. In factorial space, the coordinates of the pixels vector, on each factorial axis, are called pixels factors. The pixels factors can be considered as another multispectral image whose channels correspond to factorial axes:

$$\zeta : \left\{ \begin{array}{lcl} \mathscr{T}^L & \rightarrow & \mathscr{T}^K \,/\, K < L \\ \mathbf{f}_\lambda(x) & \rightarrow & \mathbf{c}^{\mathbf{f}}_\alpha(x) = \left(c^{\mathbf{f}}_{\alpha_1}(x), \ldots, c^{\mathbf{f}}_{\alpha_K}(x)\right) \end{array} \right. \quad (2)$$

A limited number K, with $K < L$, of factorial axes is usually chosen. Therefore FCA can be seen as a projection of initial vector pixels in a factor space with a lower dimension. Moreover, as it is shown below, FCA can be used for multispectral images to reduce noise [6, 8]. Consequently, we have two spaces for multivariate segmentation: the multispectral image space (MIS) and the factor image space (FIS). Figure 1 gives an example of a five bands satellite simulated image PLEIADES, acquired by the CNES (Centre National d'Etudes Spatiales, the French space agency) and provided by G. Flouzat [5], and its corresponding FCA representation. Its channels are the following: f_{λ_1} blue, f_{λ_2} green, f_{λ_3} red, f_{λ_4} near infrared and f_{λ_5} panchromatic. The panchromatic channel, initially of size 1460×1460 pixels with a resolution of 0.70 meters, was resized to 365×365 pixels. Therefore, the resolution is 2.80 meters in an image of $365 \times 365 \times 5$ pixels. In order to represent a multispectral image in a synthetic way, we have created a synthetic RGB image using channels f_{λ_3} red, f_{λ_2} green and f_{λ_1} blue. Figure 1 shows FCA factor pixels $\mathbf{c}^{\mathbf{f}}_{\alpha}$ of image "Roujan".

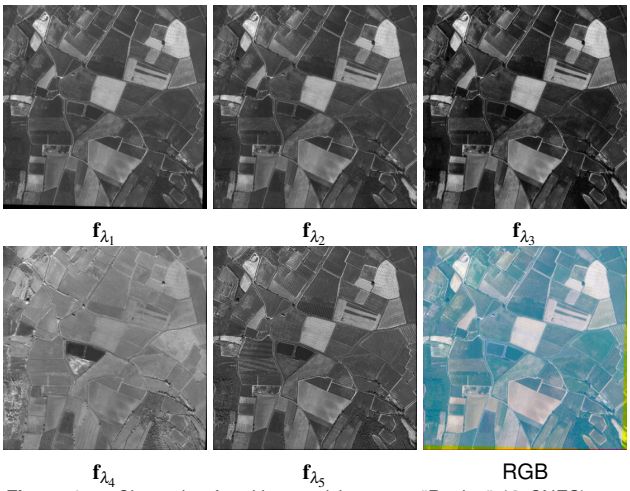

Figure 1. *Channels of multispectral image $\mathbf{f}_{\lambda}$ "Roujan" (©CNES): $\mathbf{f}_{\lambda_1}$ blue, $\mathbf{f}_{\lambda_2}$ green, $\mathbf{f}_{\lambda_3}$ red, $\mathbf{f}_{\lambda_4}$ near infra-red, $\mathbf{f}_{\lambda_5}$ panchromatic, synthetic RGB representation.*

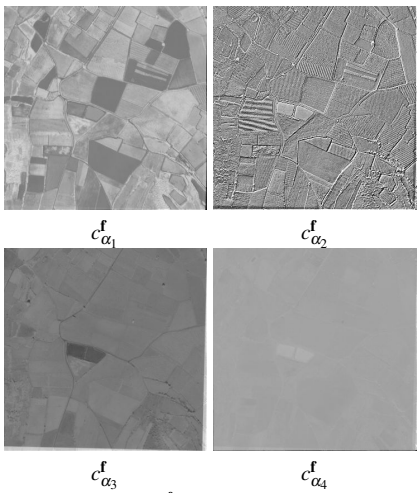

Figure 2. *FCA factors pixels $\mathbf{c}^{\mathbf{f}}_{\alpha}$ of image "Roujan" on axes 1, 2, 3 and 4 with respective inertias 84.1 %, 8.7 %, 6.2 %, 1 %.*

Pre-processing and spectral classification

As shown by Benzécri in [4] and by Green et al. in [6], some factor pixels on factor axes contain mainly noise, and others signal information. In order to choose relevant axes containing information (i.e. signal), we introduce a new method based on a measurement of signal to noise ratio SNR. For each factorial axis α_k, the centered spatial covariance is computed by a 2D FFT (Fast Fourier Transform) on the pixels factors: $\overline{g}_{\alpha_k}(h) = E[\overline{c}^{\mathbf{f}}_{\alpha_k}(x)\overline{c}^{\mathbf{f}}_{\alpha_k}(x+h)]$, with $\overline{c}^{\mathbf{f}}_{\alpha_k}(x) = c^{\mathbf{f}}_{\alpha_k}(x) - E[c^{\mathbf{f}}_{\alpha_k}(x)]$. The covariance peak, at the origin, contains the sum of the signal variance and the noise variance of the image. Then, the signal variance is estimated by the maximum (i.e. value at the origin) of the covariance $\overline{g}$ after a morphological opening γ, with a structuring element of size 3×3 pixels: $Var(signal) = \gamma\overline{g}_{\alpha_k}(0)$. In fact, one property of the morphological opening is to remove peaks on images. The noise variance is given by the residue of the opening of the covariance at the origin: $Var(noise) = \overline{g}_{\alpha_k}(0) - \gamma\overline{g}_{\alpha_k}(0)$ (fig. 3). The signal to noise ratio is defined for a factor axis as:

$$SNR_{\alpha_k} = \frac{Var(signal)}{Var(noise)} = \frac{\gamma\overline{g}_{\alpha_k}(0)}{\overline{g}_{\alpha_k}(0) - \gamma\overline{g}_{\alpha_k}(0)} \qquad (3)$$

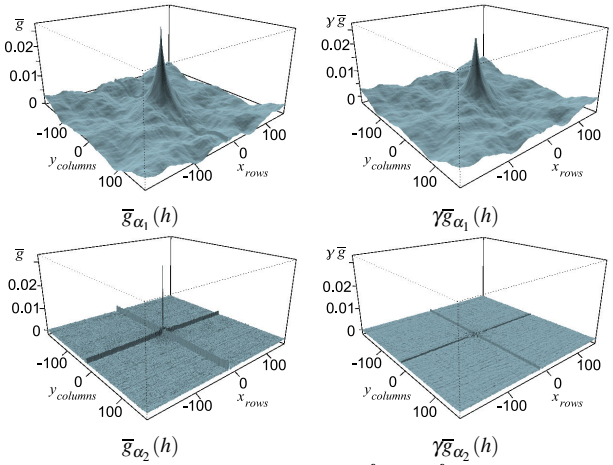

Figure 3. *2D covariances for factor pixels $c^{\mathbf{f}}_{\alpha_1}$ and $c^{\mathbf{f}}_{\alpha_2}$ of image "Roujan" before (left) and after opening (right).*

By observation of the factor pixels and their signal to noise ratios, which are higher for axes 1, $c^{\mathbf{f}}_{\alpha_1}$, and 3, $c^{\mathbf{f}}_{\alpha_3}$, than for axes 2, $c^{\mathbf{f}}_{\alpha_2}$, and 4, $c^{\mathbf{f}}_{\alpha_4}$, the axes 1 and 3 are retained.

In figure 4, we notice that axis 3, which is selected, has a lower inertia than axis 2, which is rejected. Therefore, SNR analysis makes possible to describe relevant signal, more than inertia.

After the data reduction and the spectral filtering stage by FCA, a spectral classification κ by clara [11] is performed on

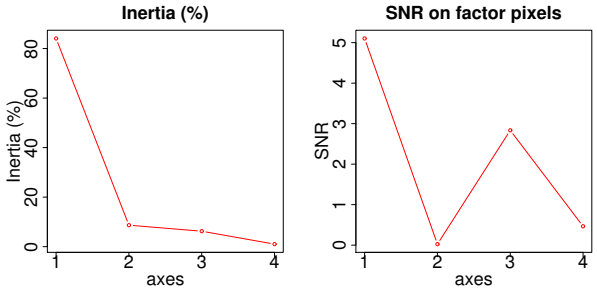

Figure 4. *Inertia (%) and SNR for factor pixels of image "Roujan".*

the factor space. We have to stress that a correct classification, used later for constructing the pdf, requires factor pixels without noise. The classification algorithm uses a euclidian distance which is coherent with the metric of the factor space [8]. The unique parameter is the number of classes, which is chosen in order to separate more the classes. Here, for this example, 3 classes are retained (fig. 5).

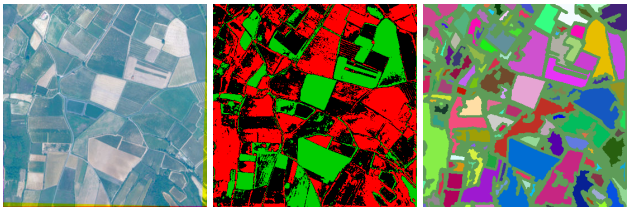

RGB κ $\widehat{\kappa}$

Figure 5. *Synthetic RGB image, classification κ in 3 classes in factor space formed by $c^{\mathbf{f}}_{\alpha_1}$ and $c^{\mathbf{f}}_{\alpha_3}$ with clara and filtered classification $\widehat{\kappa}$.*

The classification κ is then filtered class by class, in order to reduce their area. A closing by reconstruction after an erosion by a structuring element (se) of size 5×5 pixels, followed by an erosion by a se of 3×3 pixels are applied. The filtered classification is noticed $\widehat{\kappa}$.

Two reasons are available for a such filtering. First we prevent random markers from falling on the boundary of a class. In fact, during the pdf building process, in case of a leak on the channel gradient, two regions could be aggregated by a marker on the bounds of a class. The second reason is that the classes are used as seeds (i.e. markers) for the segmentation of the pdf. If all the image space E is completely full of seeds, the limits of the segmented zones are the limits of the seeds. Then, the pdf is useless. Therefore, filtering classes introduces a necessary degree of freedom for the watershed on the pdf.

Regionalized random balls markers

Regionalized random balls markers are used to build the pdf. The novelty of the paper is to condition the markers by the filtered classification $\widehat{\kappa}$.

Given $\mathscr{D} = \{D_l\}$, a partition of disjoint classes of the image space $E \subset \mathbf{R}^2$. Each class D_l of the partition is composed of connected components C_p: i.e. $D_l = \cup_p C_p$. Then the point markers μ are drawn conditionally to the connected components C_p of the filtered classification $\widehat{\kappa}$. To do this,the following rejection method is used: the point markers are uniformly distributed. If a point marker μ is inside a connected component C_p of minimum area S and not yet marked, then it is kept, otherwise it is rejected. These point markers are called regionalized random point markers.

Moreover to decrease the probability of the small, textured and low contrasted contours regions, we use random balls as markers. The centers of the balls are the regionalized random point markers and the radii r are uniformly distributed between 0 and a maximum radius $Rmax$: $\mathscr{U}[1, Rmax]$. Only the intersection between the ball $B(\mu, r)$ and the connected component C_p is kept as marker. These balls are called regionalized random balls markers.

The algorithm 1 sketches the process. We notice that N is the number of markers to be drawn. The effective number of implanted markers is less than N.

The marker image $mrk(x)$ is the union of retained markers $\mathrm{B}(\mu, r) \cap C_p$.

Algorithm 1 *Regionalized random balls markers*

Given N the number of markers to be drawn, S and $Rmax$
for all centers μ between 1 and N **do**
  if (C_p such as $\mu \in C_p$ is *not marked*) AND ($area(C_p) \geq S$) **then**
    $r = \mathscr{U}[1, Rmax]$
    keep $\mathrm{B}(\mu, r) \cap C_p$ as marker
    indicate that C_p is *marked*
  end if
end for

Probability density function

In the examples illustrating this paper, we use the weighted marginal probability density function with regionalized random balls $mpdf_{balls}$ on the image space MIS with 5 channels [9]. It would also be possible to work in the factor space FIS with a reduced number of channels. We choose to work in MIS to show that our method is not limited by the number of channels. Nevertheless, the factor space is useful for computing a correct classification used to generate the regionalized random balls markers. In the sequel, in place of using uniform random markers as in [9], regionalized random markers are thrown. The $mpdf_{balls}$ is computed as follows:

- For the morphological gradient of each channel $\rho(f_{\lambda_j})$, $j \in [1, \ldots, L]$, throw M realizations of N regionalized random balls markers, i.e. the markers $\{mrk^j_m(x)\}^{j=1\ldots L}_{m=1\ldots M}$, generating $M \times L$ realizations. Get the series of segmentations, $\{sg^j_m(x)\}^{j=1\ldots L}_{m=1\ldots M}$, by watershed associated to morphological gradients of each channel $\rho(f_{\lambda_j})$.
- Get the marginal pdf on each channel $pdf_j(x) = \frac{1}{M}\sum_{m=1}^{M} sg^j_m(x) * G_\sigma$, with G_σ a Gaussian convolution kernel ($\sigma = 3$ pixels for contours of one pixel width).
- Obtain the weighted marginal pdf $mpdf_{balls}(x) = \sum_{j=1}^{L} w_j pdf_j(x)$, with $w_j = 1/L$, $j \in [1, \ldots, L]$ in MIS and w_j equal to the inertia axes in FIS.

Some markers and their associated realizations of contours are presented in figure 6. The pdf $mpdf_{balls}$ is shown in figure 7.

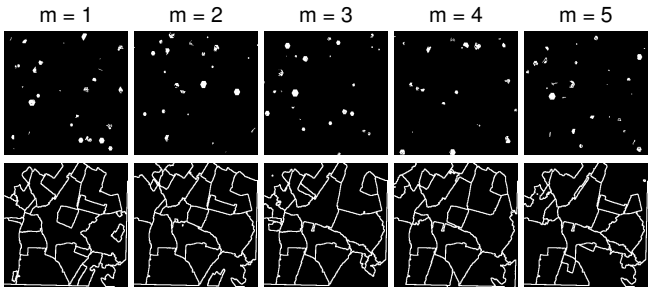

Figure 6. *A few realizations of regionalized random balls markers $\{mrk^j_m(x)\}^{j=1}_{m=1\ldots5}$ (top) by the classification $\widehat{\kappa}$ and associated contours of watershed $\{sg^j_m(x)\}^{j=1}_{m=1\ldots5}$ (bottom).*

Segmentation

For segmentation, we compare a deterministic and a stochastic approach on multivariate images (fig. 7).

First step : For both cases, an unsupervised classification κ (kmeans or "clara") is processed in factor space FIS and filtered $\widehat{\kappa}$.

Second step :

- For the deterministic approach, a chi-squared metric based gradient $\rho^{\chi^2}(\mathbf{f}_\lambda)$ is computed in image space MIS, as a function to flood [8].
- For the stochastic approach, a marginal probability density function $mpdf_{balls}$, with regionalized random balls markers conditioned by the filtered classification $\widehat{\kappa}$, is processed, in image space MIS, as a function to flood [9].

Third step : In both cases, the flooding function is segmented by a watershed (WS) using as sources of flooding the seeds from the filtered classification $\widehat{\kappa}$.

The results are images segmented by stochastic WS with seeds from classification $WS^{\widehat{\kappa}}_{sto.balls}$ and deterministic WS with seeds from classification $WS^{\widehat{\kappa}}_{det}$.

Results

In figure 7, are given the results of segmentation by deterministic and stochastic WS for image "Roujan" with seeds coming from filtered classification $\widehat{\kappa}$. We observe that the contours are smoother and follows more the main limits of the regions for the stochastic approach than for the deterministic one. The parameters for the stochastic WS with seeds coming from the classification $WS^{\widehat{\kappa}}_{sto.balls}$ are:

- the number of classes for the classification κ: $Q = 3$;
- the maximum number of random balls markers: $N = 50$, which corresponds to the same order of the number regions in the image ;
- the number of realizations for each channel: $M = 100$, always the same ;
- the minimum area $S = 10$ pixels for connected classes C_p, generally the same ;
- the maximum radius of the random balls $Rmax = 30$, generally the same.

In figure 8, for comparison with a segmentation based on a prior number of regions, other images, similar to image "Roujan", are segmented: "Roujan 0 2 " and "Roujan 1 9". As for image "Roujan", factor axes $c^{\mathbf{f}}_{\alpha_1}$ and $c^{\mathbf{f}}_{\alpha_3}$ are kept. They present both a higher SNR than the other axes. Inertias and SNR for factor axes of images "Roujan X X" are presented on the following tables.

A classification "clara" is computed on the factor pixels of these two axes. The $mpdf_{balls}$ are produced as explained for image "Roujan".

Inertia for factor axes for images "Roujan X X"

Image	$c^{\mathbf{f}}_{\alpha_1}$	$c^{\mathbf{f}}_{\alpha_2}$	$c^{\mathbf{f}}_{\alpha_3}$	$c^{\mathbf{f}}_{\alpha_4}$
"Roujan"	84.1 %	8.7 %	6.2 %	1 %
"Roujan 0 2"	75.6 %	13.7 %	9.2 %	1.5 %
"Roujan 1 9"	77.5 %	12.1 %	9 %	1.4 %

SNR for factor axes for images "Roujan X X"

Image	$c^{\mathbf{f}}_{\alpha_1}$	$c^{\mathbf{f}}_{\alpha_2}$	$c^{\mathbf{f}}_{\alpha_3}$	$c^{\mathbf{f}}_{\alpha_4}$
"Roujan"	5.10	0.03	2.84	0.47
"Roujan 0 2"	2.66	0.01	2.53	0.32
"Roujan 1 9"	3.15	0	2.90	0.51

To segment these $mpdf_{balls}$ two methods are compared:

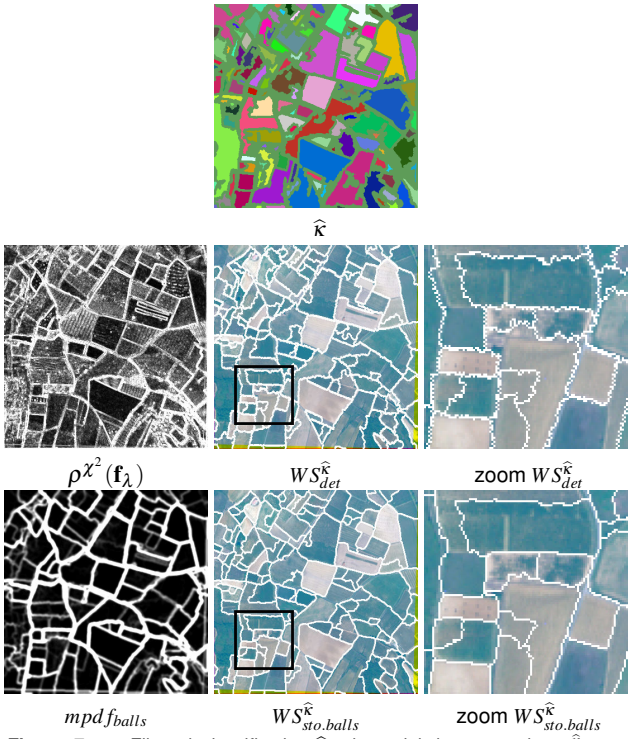

Figure 7. *Filtered classification $\widehat{\kappa}$, deterministic approach $WS^{\widehat{\kappa}}_{det}$ on Chi-squared metric based gradient $\rho^{\chi^2}(\mathbf{f}_\lambda)$ (top) and stochastic approach $WS^{\widehat{\kappa}}_{sto.balls}$ on $mpdf_{balls}$ (bottom) on image "Roujan". In both cases, the seeds come from $\widehat{\kappa}$. For visualization, and for complete segmented images the contours are dilated by a se of size 3×3 pixels.*

- a WS with seeds coming from the filtered classification $WS^{\widehat{\kappa}}_{sto.balls}$;
- a hierarchical WS based on extinction values, which allows to select the minima according to a morphological criterion of volume $WS^{vol}_{sto.balls}$.

In figure 8, we notice that the number of regions, resulting from the segmentation, strongly depends on the image, whereas the number of classes is the same for similar images. In fact, the number of regions for volumic WS, $WS^{vol}_{sto.balls}$, must be chosen according to the considered image, and cannot be fixed "a priori" (50 here). The number of regions depends on the size and the complexity of the image, while the number of classes depends on the spectral content. Consequently, it is more relevant to use a WS with seeds coming from the classification $WS^{\widehat{\kappa}}_{sto.balls}$. Moreover only one parameter is needed for WS with seeds $WS^{\widehat{\kappa}}_{sto.balls}$: the number of classes in the classification. This parameter is the same for similar images and can be chosen more easily than the number of regions. Moreover, the number of classes produces a more robust segmentation than the number of regions.

Some other results are presented on image "Port de Bouc", in figure 9. Two factor axes are retained in FIS: $c^{\mathbf{f}}_{\alpha_1}$ and $c^{\mathbf{f}}_{\alpha_2}$ of respective inertias: 60.1 % and 23.4 % and of respective SNR: 18.7 and 3.16. The parameters for the stochastic WS are: $Q = 7$ classes for the classification κ, $N = 100$ random balls at maximum, $M = 100$ realizations, a minimum area of $S = 10$ pixels for the connected classes C_p and a maximum radius of $Rmax = 30$ pixel for random balls. We notice that contours are more regular for stochastic WS than for deterministic WS.

One of the main artefacts of deterministic watershed is that small regions strongly depend on the position of the markers, or on the volume, i.e. the integral of the gray levels of the catch-

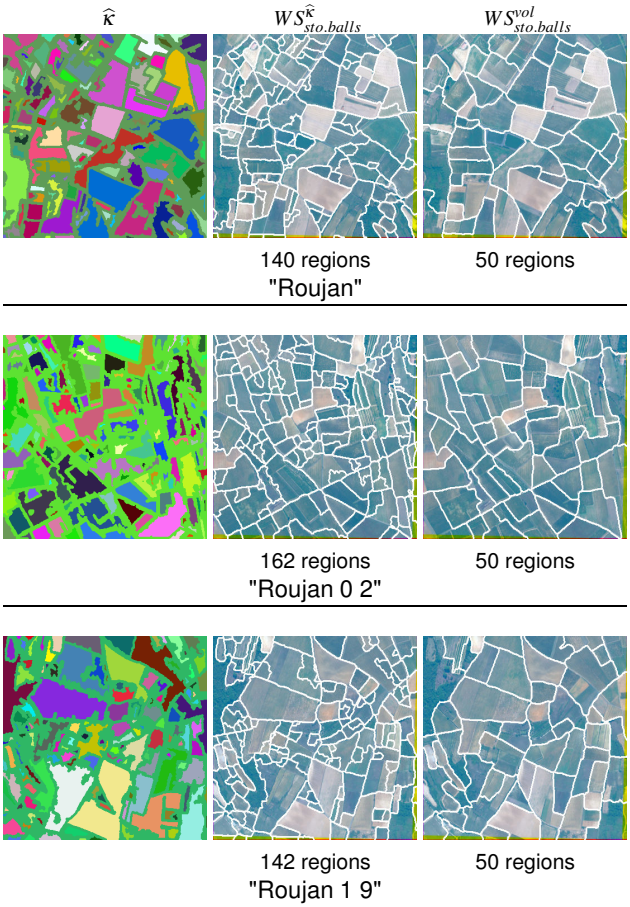

Figure 8. *Comparison between segmentations of $mpdf_{balls}$ by stochastic WS with a prior given number of regions $R = 50$ ($WS^{vol}_{sto.balls}$) or with seeds coming from the filtered classification $WS^{\widehat{\kappa}}_{sto.balls}$. The results are given for images: "Roujan", "Roujan 0 2", "Roujan 1 9".*

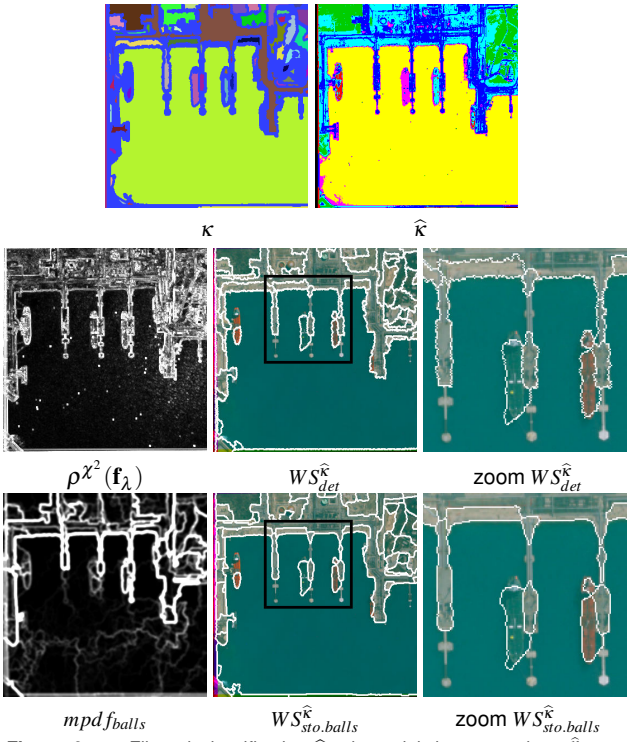

Figure 9. *Filtered classification $\widehat{\kappa}$, deterministic approach $WS^{\widehat{\kappa}}_{det}$ on Chi-squared metric based gradient $\rho^{\chi^2}(\mathbf{f}_\lambda)$ (top) and stochastic approach $WS^{\widehat{\kappa}}_{sto.balls}$ on $mpdf_{balls}$ (bottom) on image "Port de Bouc". In both cases, the seeds come from $\widehat{\kappa}$. For visualization, and for complete segmented images the contours are dilated by a se of size 3×3 pixels.*

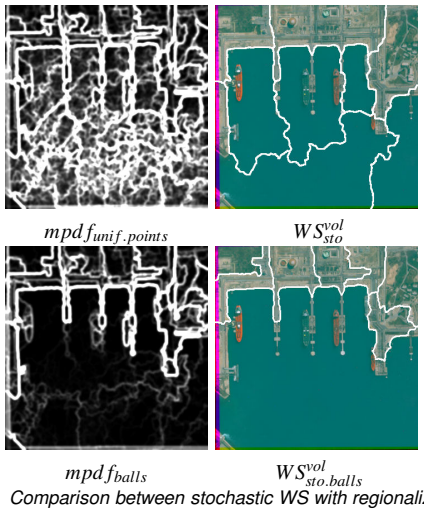

Figure 10. *Comparison between stochastic WS with regionalized random balls markers with a volume criterion $WS^{vol}_{sto.balls}$ to the stochastic WS with uniform random points markers with a volume criterion WS^{vol}_{sto}. There are $R = 8$ regions. For visualization, and for complete segmented images the contours are dilated by a se of size 3×3 pixels.*

ment basin, associated to their minima. In fact, there are two kinds of contours associated to the watershed of a deterministic gradient such as $\rho^{\chi^2}(\mathbf{f}_\lambda)$: 1st order contours, which correspond to significant regions and which are relatively independent from markers; and 2nd order contours, associated to "small", "low" contrasted or textured regions, which depend strongly on the location of markers. Stochastic watershed aims at enhancing the 1st order contours from a sampling effect, to improve the resulting segmentations.

Therefore even with good markers, obtained from classification for multispectral images, the contours of the stochastic WS are more regular than for deterministic WS.

Moreover, we have compared the stochastic WS with regionalized random balls markers with a volume criterion $WS^{vol}_{sto.balls}$, presented in this paper, to the stochastic WS with uniform random points markers with a volume criterion WS^{vol}_{sto}, presented in [9]. The number of regions is $R = 8$ (fig. 10). We notice that $WS^{vol}_{sto.balls}$ concentrates more on main contours of the image than WS^{vol}_{sto} especially for the part concerning the sea. Therefore, stochastic WS with regionalized random balls markers $WS^{vol}_{sto.balls}$ improves the result of stochastic WS with uniform random point markers WS^{vol}_{sto}.

Conclusions and perspectives

In this paper we have introduced a new way of computing regionalized random markers introducing spectral information in the weighted marginal probability density function $mpdf_{balls}$. Therefore, $mpdf_{balls}$ contains now spectral and spatial information. Usually the main difficulty is the choice of the number of regions for the segmentation. Here, we have presented a complete treatment chain for segmenting multispectral images with a major and robust parameter: the number of classes of the classification. We have shown that the number of classes for the classification is more robust than the number of regions for the segmentation. Moreover, even with good markers, obtained by classification for multispectral images, the contours of the final segmentation are smoother for the stochastic WS with seeds coming

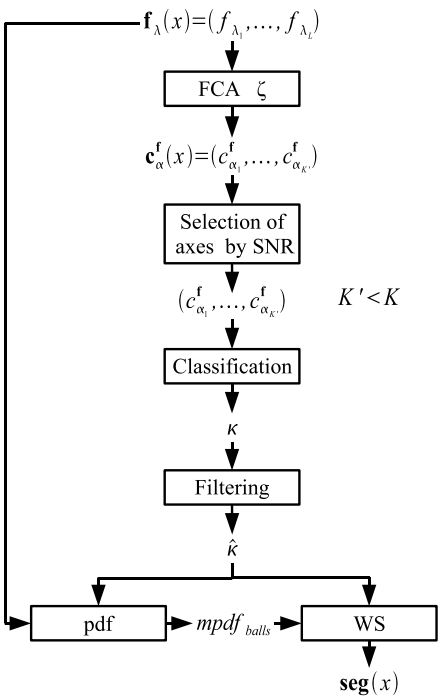

Figure 11. *Complete flowchart for classification-driven stochastic WS with regionalized random balls markers* $WS^{\hat{\kappa}}_{sto.balls}$.

from the classification, than for the deterministic WS with the same seeds.

Finally, we have introduced a general methodology for segmenting multispectral images. We are thinking on applying on different fields are numerous: medical images [10], microscopy images, thermal images, temporal series, multivariate series, etc.

Acknowledgments

The authors are grateful to Prof. Guy Flouzat (Laboratoire de Télédétection à Haute Résolution, LTHR/ ERT 43 / UPS, Université Paul Sabatier, Toulouse 3, France) for his collaboration on PLEIADES satellite simulated images in the framework of ORFEO program (Centre National d'Etudes Spatiales, the French space agency).

References

[1] J. Angulo, D. Jeulin, Stochastic watershed segmentation, Proc. Int. Symp. Mathematical Morphology ISMM'07 Rio, Brazil, INPE, Eds. Banon, G. et al., pg. 265–276 (2007).

[2] S. Beucher, F. Meyer, The Morphological Approach to Segmentation: The Watershed Transformation, Mathematical Morphology in Image Processing, Marcel Dekker, Eds. E. Dougherty, 1992, pg. 433—481.

[3] S. Beucher, Watershed, hierarchical segmentation and waterfall algorithm, Proc. Int. Symp. Mathematical Morphology ISMM'94, pg. 69–76 (1994).

[4] J.P. Benzécri, L'Analyse Des Données. L'Analyse des Correspondances II, Paris, Dunod, 1973, pg. 1–166.

[5] F. Laporterie-Déjean, H. De Boissezon, G. Flouzat, M.J. Lefèvre-Fonollosa, Thematic and statistical evaluations of five panchromatic/multispectral fusion methods on simulated PLEIADES-HR images, Information Fusion, 6, 193–212 (2005).

[6] A.A. Green, M. Berman, P. Switzer, M.D. Craig, A Transformation for Ordering Multispectral Data in terms of Image Quality with Implications for Noise Removal, IEEE Trans. Geosc. Rem. Sens., 26, 65–74 (1988).

[7] F. Meyer: An overview of Morphological Segmentation, International Journal of Pattern Recognition and Artificial Intelligence, 15 (7), 1089–1118 (2001).

[8] G. Noyel, J. Angulo, D. Jeulin, Morphological Segmentation of hyperspectral images, Image Analysis and Stereology, 26, 101–109 (2007).

[9] G. Noyel, J. Angulo, D. Jeulin, Random Germs and Stochastic Watershed for Unsupervised Multispectral Image Segmentation. Proc. KES 2007/ WIRN 2007, Part III, LNAI 4694, Springer, pg. 17-–24 (2007).

[10] G. Noyel, J. Angulo, D. Jeulin, D. Balvay, CA. Cuenod, Filtering, segmentation and region classification by hyperspectral mathematical morphology of DCE-MRI series for angiogenesis imaging. Internal note N-02/08/MM, Ecole des Mines de Paris. Accepted at ISBI 2008, IEEE International Symposium on Biomedical Imaging, Paris, France, May 14-17 (2008).

[11] L. Kaufman, P.J. Rousseeuw, Finding Groups in Data. An Introduction to Cluster Analysis, Ch. 2 and 3, John Wiley and Sons, 1990, pg. 28–160.

Author Biography

Guillaume NOYEL is a PhD student at the Centre de Morphologie Mathématique of Ecole des Mines de Paris. He receives his Master degree in Image processing in 2005 from CPE-Lyon, France and his MSc in Image processing (with honors) in 2005 from University J. Monnet, St Etienne, France. His research fields are segmentation, data reduction of hyperspectral images and mathematical morphology. The applications are in biomedicine, remote sensing and temporal series.

Jesús ANGULO received a degree in Telecommunications Engineering (1999). He obtained his PhD in Mathematical Morphology and Image Processing (2003), from the Ecole des Mines de Paris (ENSMP). He is currently a researcher in the Center of Mathematical Morphology of ENSMP. His research interests are in the areas of multivariate image processing (colour, hyper/multi-spectral, temporal series, tensor imaging) and mathematical morphology, and their applications to biomedicine and biotechnology.

Dominique JEULIN is Director of Research and Professor in Ecole des Mines de Paris. At the head of the "Physics of Heterogeneous Media" group, his main current interest covers the theoretical prediction of physical properties of random media (fracture statistics models, homogenization of mechanical and optical properties of composite materials and of biological tissues), models and simulations of random media, 3D image analysis, applications to Materials Science, Biology and Vision.